NORSAR Scientific Report No. 1-2013

# Semiannual Technical Summary

1 January – 30 June 2013

Tormod Kværna (Ed.)

Kjeller, December 2013

# 6 Technical Reports / Papers Published

## 6.1 An Application of Coda Envelopes for Estimation of Stable Event Magnitudes in Southern Norway

### 6.1.1 Introduction: motivation and study area

In seismology, applications like the determination of seismic hazard require accurate and reliable magnitude estimates. Previous studies (*e.g.*, Ringdal, 1983; Ringdal and Hokland, 1987; Mayeda and Walter, 1996) have shown that coda amplitude measurements have significantly less variability than measurements of direct wave amplitudes. This property of coda permits an alternative approach in magnitude estimation. It has been demonstrated in several papers (e.g., Mayeda et al., 2003; Eken et al., 2004; Morasca et al., 2005; Morasca et al., 2008) that stable estimates of source moment spectra can be derived from regional coda envelopes observed at only 1-3 stations.

The objective of this study is to test the coda-based method for magnitude estimation at regional distances using broadband and short-period stations located in Norway. Initially, we address the NORSAR array (NOA), which when calibrated, could permit re-estimation of event magnitudes based on coda derived moment source spectra for the large number of events found in its digital archive. Furthermore, two additional stations (BER and AKN) are calibrated in order to evaluate the consistency of our results.

Coda techniques were first developed for local network data using the late coda. This allowed the coda wavefield to homogenize and therefore to be less dependent on a particular travel path and to be less sensitive to source radiation effects. However at regional distances the late coda is measurable only for large events. Mayeda et al., 2003 developed a new technique to analyze coda at regional distance by measuring earlier sections of the coda by introducing corrections for distance dependence effects. Our methodology is mainly based on the “Mayeda” method and consists of the following calibration steps: coda window selection, coda shape calibration, distance normalization, site-response correction using the smaller events as Green's functions, and conversion of the non-dimensional spectra to absolute source spectra using independent moment estimates for the largest events.

In this study, the three stations AKN, BER and NOA are calibrated (see Fig. 6.1.1). Our data set consists mainly of small events with local magnitudes between 1.5 and 3.5 located in the western part of southern Norway (see Appendix for event characteristics). From 2009, seventeen of the largest events had independent seismic moment magnitude estimates reported in the University of Bergen seismic event catalog ($M_W$*(BER)*).

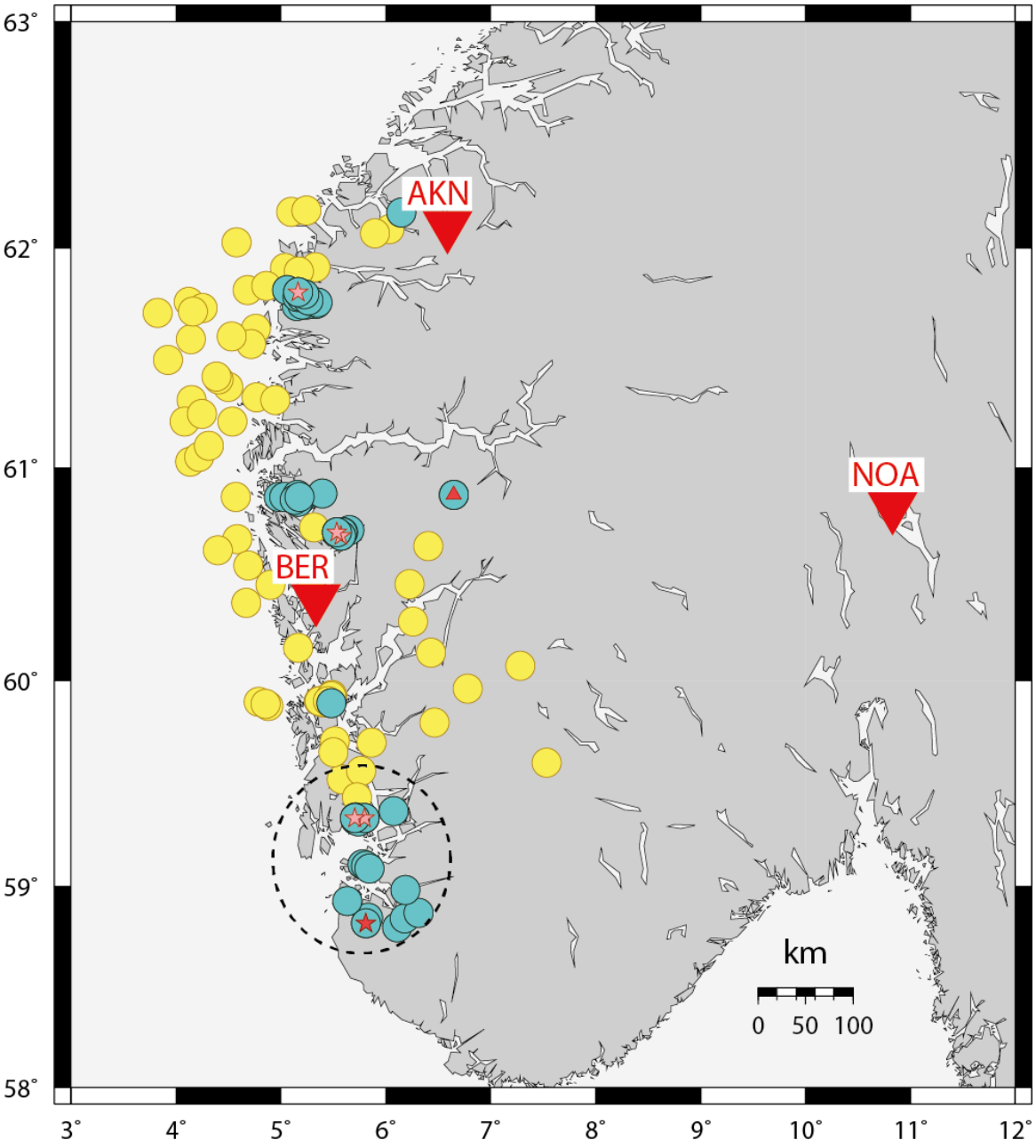


*Fig 6.1.1 Stations (red inverted triangles) and events (filled circles) used in this study. BER and AKN are two single broadband stations, and NOA is an array of short period and broadband stations. Yellow circles correspond to events with normal coda derived source spectra and blue circles to events with anomalous coda derived source spectra. See section 6.1.3 for more details. Small symbols inside the filled circles correspond to events which were reported to be landsides (red triangles), or, confirmed (red stars) and probable explosions (pink stars) according to the University of Bergen catalog. The dotted circle in southwestern Norway indicate an area where we had selected a few events for comparison of spectra from explosions and earthquakes (see Fig. 6.1.9).*

### 6.1.2 Methodology

#### *6.1.2.1* Formation *of coda envelopes*

The raw data is converted into ground velocity. Then coda envelopes for 12 narrow frequency bands are formed using the equation below:

$$Env(fi,t) = |(x_{fi}(t) + i \times H(x_{fi}(t))| \quad (1)$$

where $fi$ is the center frequency of narrow frequency bands, $t$ the time relative to the origin, $x_{fi}$ the filtered seismogram and $H$ its Hilbert transform.

The envelopes are smoothed with a Hanning window using the envelope parameters given in Table 6.1.1. To provide smoother envelopes, it is possible to stack the envelopes from short-period array stations. That is why we choose in this study to stack the envelopes of the 6 vertical-component sensors of sub-array NB2 to represent the coda of the large-aperture NORSAR (NOA) array. An example of smoothed coda envelopes at NB2 is shown in Fig. 6.1.2.

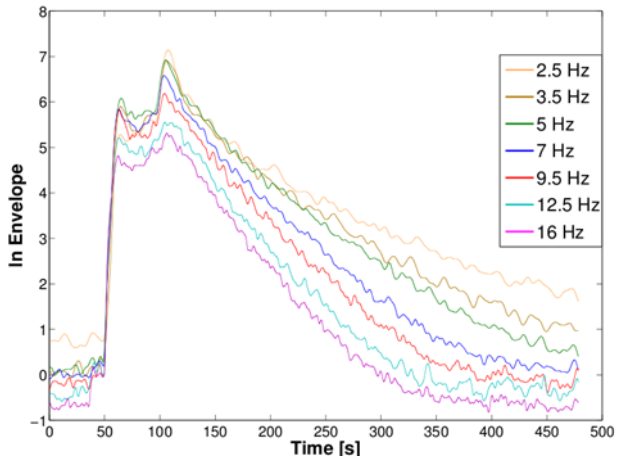


*Fig. 6.1.2*
*Example of selected observed NOA narrowband envelopes of a magnitude 3 earthquake occurring on 22 March 2013, located at a distance of 350 km from the station (see event information in the Appendix). We can see strong frequency dependency in the shape of the coda envelopes. That is why we must define the parameters of the coda shape as a function of frequency.*

The analytic expression of the narrowband coda envelopes that we used to fit with the observed ones is defined as follows (Mayeda *et al.*, 2003)**:**

$$A(f_i,t,r) = W(f_i)S(f_i)\ \overbrace{P(f_i,r)\underbrace{(t-t_S)^{-\gamma}e^{b(f_i)(t-t_S)}}_{\text{Coda Shape function}}}^{\textbf{Propagation term}} H(t-t_s) \quad (2)$$

where $f_i$ is the center frequency of the narrowband envelope, $t$ the time from origin, $r$ the epicentral distance, $t_S$ the direct S-wave travel time, $\gamma$ and $b$ the coda shape parameters, $H$ the Heaviside function, $W(f_i)$ the S-wave source amplitude, $S(f_i)$ the site response and $P(f_i,r)$ the distance effect. To obtain the source spectra, we remove all the propagation and site effects over all frequency bands.

***Table 6.1.1 Coda calibration parameters***

| Envelopes parameters | | | Shape parameters | | | | Normalization | Site response correction parameter | | | Moment conversion parameter | | |
|---|---|---|---|---|---|---|---|---|---|---|---|---|---|
| Fi (Hz) | Width (Hz) | Smoother Width (s) | γ | b | | | Tnorm (s) | ln(S) | | | $M_p$ | | |
| | | | | AKN | BER | NOA | | AKN | BER | NOA | AKN | BER | NOA |
| 0.4 | 0.2 | 32 | 0.5 | - | - | - | 500 | - | - | - | 20.25 | 20.97 | 20.18 |
| 0.6 | 0.2 | 26 | 0.5 | - | - | - | 500 | - | - | - | 20.25 | 20.97 | 20.18 |
| 0.85 | 0.3 | 22 | 0.5 | -0.0059 | -0.0098 | -0.0044 | 500 | 0 | 0 | 0 | 20.25 | 20.97 | 20.18 |
| 1.25 | 0.5 | 18 | 0.5 | -0.0071 | -0.0028 | -0.0072 | 500 | -0.282 | 3.067 | -0.610 | 20.25 | 20.97 | 20.18 |
| 1.75 | 0.5 | 15 | 0.5 | -0.0078 | -0.0093 | -0.0073 | 500 | -0.537 | 0.562 | -0.623 | 20.25 | 20.97 | 20.18 |
| 2.5 | 1 | 13 | 0.5 | -0.0098 | -0.0065 | -0.0091 | 500 | -0.964 | 2.063 | -0.879 | 20.25 | 20.97 | 20.18 |
| 3.5 | 1 | 11 | 0.5 | -0.0123 | -0.0121 | -0.0110 | 500 | -1.766 | -0.063 | -1.607 | 20.25 | 20.97 | 20.18 |
| 5 | 2 | 9 | 0.5 | -0.0173 | -0.0137 | -0.0131 | 500 | -2.982 | -0.407 | -2.176 | 20.25 | 20.97 | 20.18 |
| 7 | 2 | 8 | 0.5 | -0.0189 | -0.0158 | -0.0153 | 500 | -3.249 | -1.161 | -3.176 | 20.25 | 20.97 | 20.18 |
| 9.5 | 3 | 6 | 0.5 | -0.0202 | -0.0150 | -0.0169 | 500 | -3.602 | -0.603 | -3.825 | 20.25 | 20.97 | 20.18 |
| 12.5 | 3 | 6 | 0.5 | -0.0203 | -0.0187 | -0.0179 | 500 | -4.347 | -2.353 | -4.471 | 20.25 | 20.97 | 20.18 |
| 16 | 4 | 5 | 0.5 | -0.0233 | -0.0181 | -0.0185 | 500 | -5.708 | -2.145 | -4.829 | 20.25 | 20.97 | 20.18 |

### *6.1.2.2 Coda window selection*

The analytic expression of the coda envelope given in equation (2) is defined for times greater than the direct S-wave arrival $t_S$. In order to automatically align the observed and synthetic envelopes, we define the time of the direct S-wave arrival $t_S$ as the time identified by the envelope's peak amplitude. This definition of the direct S-wave arrival associates the coda with different phases, most often the $L_g$ phase, but also the $S_n$ phase (see Fig. 6.1.3).

As we expect a group velocity for S waves ($L_g$,$S_n$) around 3.5 km/s, we look for the envelope's peak amplitude in the time interval where the group velocity is between 2 and 4 km/s. Then, the coda window is selected manually for each frequency. But pre-selected extreme limits are defined for helping the user: the default left limit of the coda window corresponds to the direct S-wave arrival and the default right limit is when the signal to noise ratio is falling below a predefined threshold.

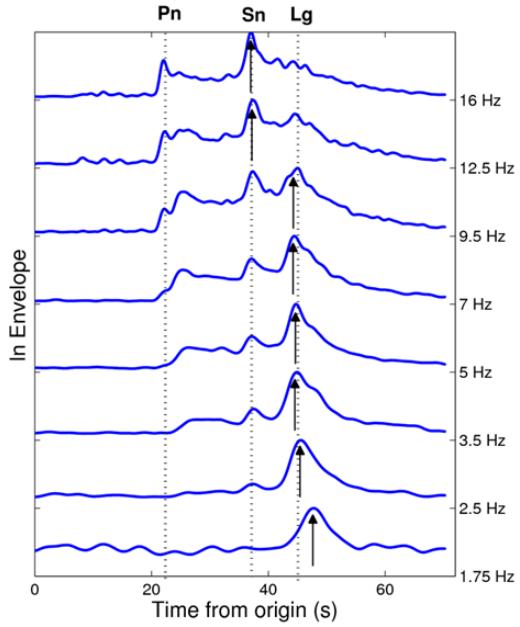


*Fig. 6.1.3*
*Example of selected narrowband envelopes of a magnitude 2 earthquake recorded by NOA. The event occurred on 25 December 2011 at a distance of 380 km from the station (see Appendix). The arrows show the envelope peak amplitude for each frequency. We can note the shift from $L_g$ to $S_n$ coda for the higher frequencies.*

### *6.1.2.3 Create Synthetic envelopes: coda shape calibration, distance normalization*

a) Coda shape Parameter

By taking the logarithm of equation (2) we obtain for a fixed frequency $f_i$:

$$\ln(A(f_i,t,r)(t-t_S)^{\gamma}) = \underbrace{\ln(W(f_i)\,S(f_i)P(f_i,r))}_{\textbf{Time independent}} + b(t-t_S) \qquad (3)$$

Thus, we can obtain $b$ by linear regression by fixing $\gamma$. Aki and Chouet (1975) showed that the difficulty to exactly define when the coda window starts explains the erratic behavior of the coefficient $\gamma$ when it is estimated from the data. That is why we chose to fix $\gamma$ instead of estimating it from the data by using a grid-search. Aki and Chouet (1975) suggest two extreme models of coda waves: a single scattering model ($\gamma = 0.5$ or $1$ for surface wave or body wave) and a diffusive model ($\gamma = 0.75$). According to the regional distances in this study (100-400km) we expect more surface waves, so we chose to fix $\gamma = 0.5$.

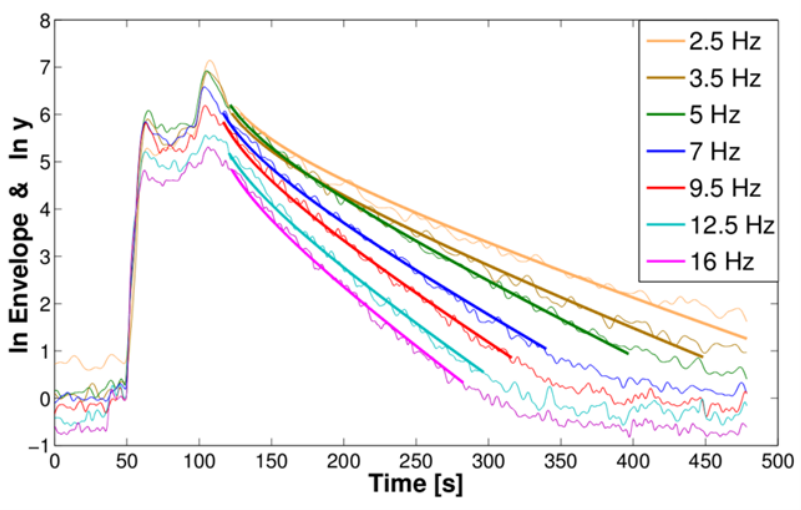


*Fig. 6.1.4*
*Example of selected observed narrowband envelopes (thin lines) of the magnitude 3 earthquake recorded at NOA (see also Fig. 6.1.2). Bold lines show synthetic coda shape fits using equation (3):*
$ln\, y = -\gamma\ ln(t - t_S) + b(t - t_S) + ln(WSP)$

Fig. 6.1.4 shows an example of coda envelopes of an event used for the calibration with the associated synthetic coda shape estimated by linear regression for ɣ equal to 0.5. We can now determine the coda shape parameters as a function of frequency for the selected region by simply averaging the estimated coda shape parameters from a subset of events. Table 6.1.1 gives the estimated coda shape parameters for the studied area. We chose events which had independent seismic moment magnitude estimates in order to have the same subset for each step of the calibration, and also because these events have a good signal-to-noise ratio.

b) Distance normalization

At this point, we have determined the coda shape function. The near-regional coda energy appears to be homogeneously distributed. Fig 6.1.5.a illustrates this by using three events which have approximately the same magnitude ($2.2<M_L<2.3$), but being located at different distances from the recording station AKN, i.e., 120 km, 180 km and 250 km, respectively. The observed coda envelopes attain roughly the same level and shape at larger lapse times. However, the coda shape functions shown in Fig. 6.1.5.b show different amplitude levels, revealing a distance-dependence. The two approaches for estimating distances corrections proposed by Mayeda *et al*. (2003), using a source normalization or a simultaneous grid search, are not feasible. This is because we do not have a sufficiently large number of events in our database with a narrow magnitude range spanning a range of distances, or common events observed at two stations that span a range of distances. We therefore decided to use the observation at large lapse times to correct the synthetic envelopes coda for distance dependence. We simply normalize the synthetic envelopes at a fixed large lapse time (500 seconds) in order to overlay the envelopes at large lapse time and mimic the real behavior as proposed by Morasca *et al.* (2005). The distance normalized envelopes are shown in Fig. 6.1.5.c.

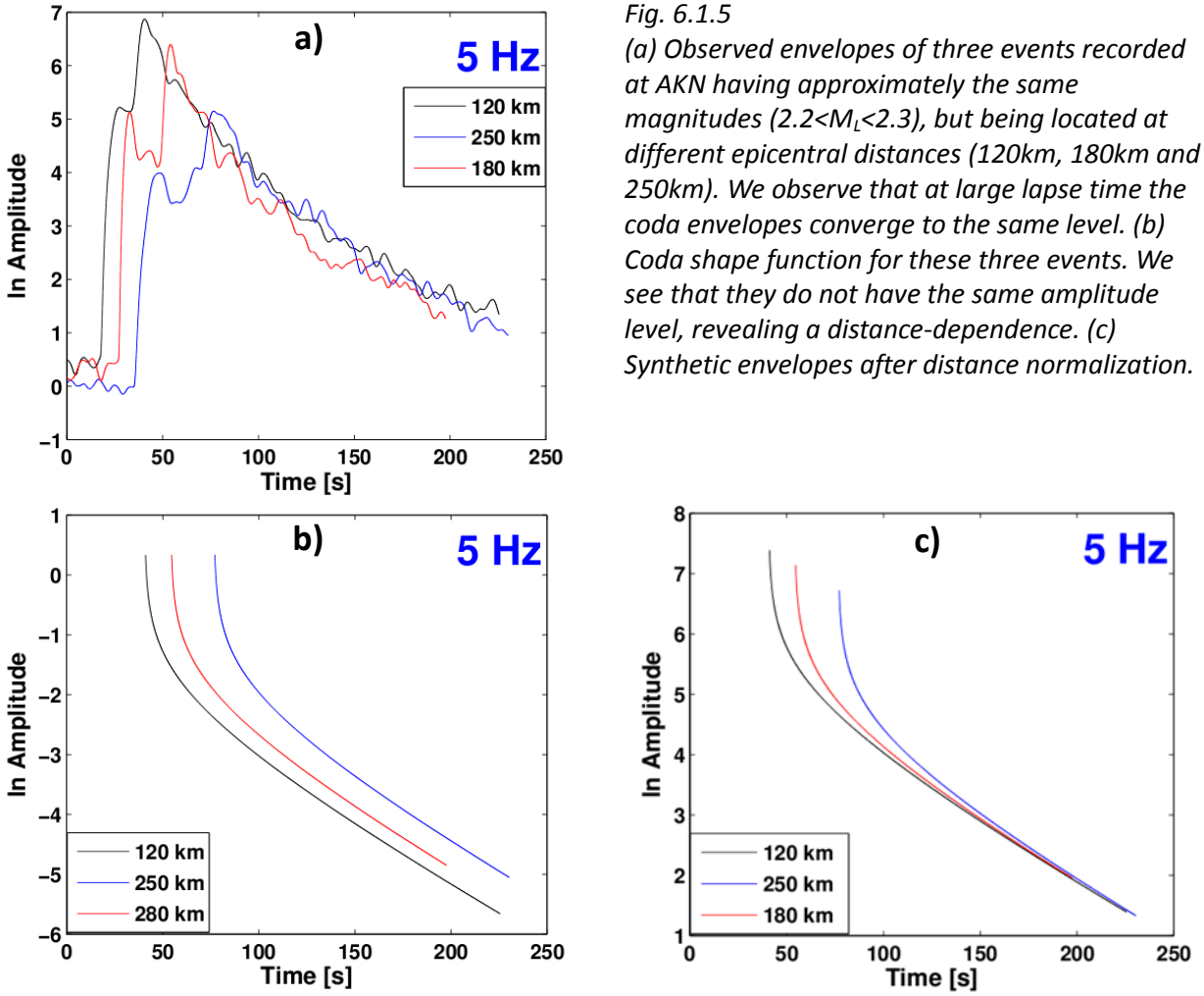


*Fig. 6.1.5*
*(a) Observed envelopes of three events recorded at AKN having approximately the same magnitudes (2.2<$M_L$<2.3), but being located at different epicentral distances (120km, 180km and 250km). We observe that at large lapse time the coda envelopes converge to the same level. (b) Coda shape function for these three events. We see that they do not have the same amplitude level, revealing a distance-dependence. (c) Synthetic envelopes after distance normalization.*

c) Coda amplitude measurement

The distance corrected synthetic envelopes are then used to measure the coda amplitude of the observed envelopes by vertically shifting the synthetics until they fit the observed ones.

### *6.1.2.4 Site response correction*

At this point, we can measure distance-corrected coda amplitude from narrowband envelopes, which includes both the source and site effects. So, we need to correct the amplitude measurement by the site effect to obtain the source term. We used the procedure outlined by Mayeda *et al.* (2003) which assumes that the S-wave source spectrum is flat below the corner frequency (see Fig. 6.1.6). The corner frequency for each event is estimated according to local magnitudes in the Bergen catalog using a model of source spectrum for an input stress drop of 3 MPa.

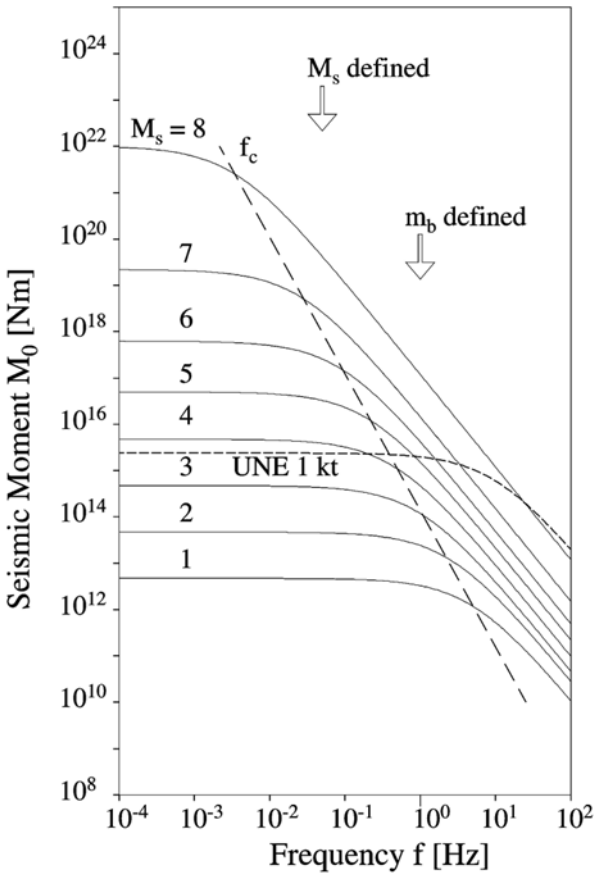


*Fig. 6.1.6*
*Extracted from Bormann (2002). Source spectra of ground displacement for a seismic shear source for different magnitudes. Source spectra are characterized by a plateau of constant displacement spectral amplitudes for frequencies smaller than the corner frequency $f_c$ and a decay of spectral displacement amplitude proportional to $f^{-2}$ for frequencies above the corner frequency. The long-dashed line shows the increase of corner frequency with decreasing seismic moment of the event.*

We apply a correction to each frequency band that flattens the portion of the source spectrum for frequencies below the estimated corner. Because of the increase of corner frequency with decreasing magnitude, the smaller events are used as empirical Green's functions to derive corrections for all events for each frequency. The corrections used to flatten the smaller events are also applied to the larger events (Fig. 6.1.7). We obtain after correction dimensionless coda-derived spectra.

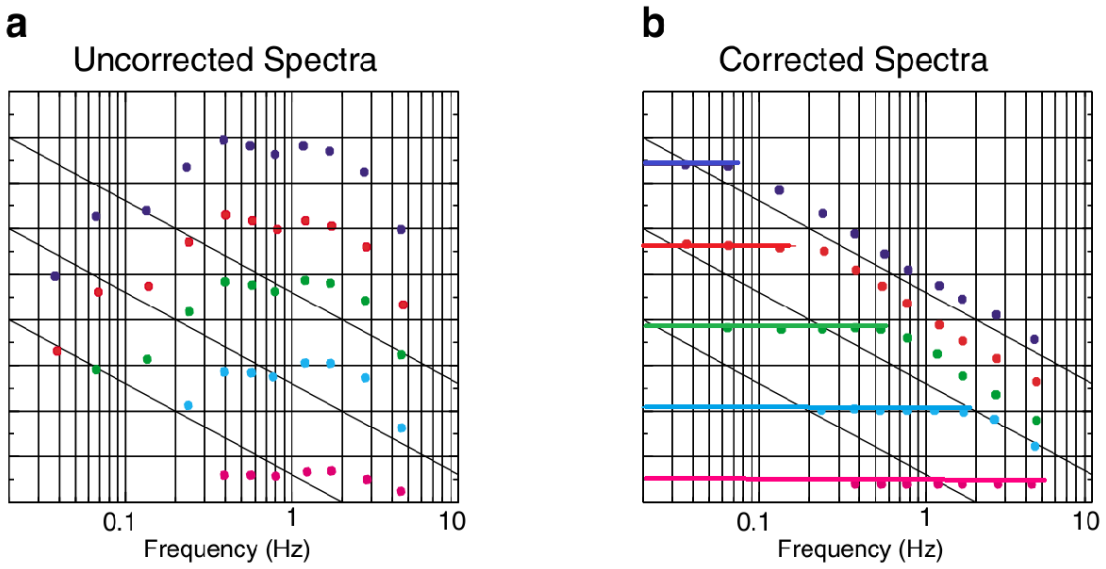


*Fig. 6.1.7 Figure illustrating the site response correction (adopted from Mayeda at al., 2003). (a) Distance corrected coda amplitude before correction. (b) Distance corrected coda amplitude after correction. Bold solid lines show that the applied corrections flatten the portion of source spectrum for frequencies below the estimated corner frequency. The diagonal black lines have a slope proportional to $f^{-2}$. We assume that the coda amplitude decay fits this slope for frequencies above the corner frequency.*

### *6.1.2.5 Tying the source spectra to an absolute scale*

In order to tie our dimensionless spectra to an absolute scale, we use a linear relation between our dimensionless coda-derived moment $A_0$ (which is the mean value of distance-site effect corrected coda amplitude (*CorrAmp*) for frequencies below the estimated corner frequency $f_c$ and the estimated seismic moment $M_0$ using independent moment magnitudes ($M_w$) given in the Bergen catalog:

$$\log_{10} A_0 = mean_{f_i < f_c} \left( \log_{10} CorrAmp(f_i) \right) \quad \text{[Dimensionless units]} \quad (4)$$

$$\log_{10} M_0 = \frac{3}{2}(M_w + 10.75) \quad [\log_{10}\text{dyne-cm}] \text{ [Hanks and Kanamori 1979]}$$

We obtain the moment conversion parameter $M_p$ using our subset of 17 events with independently determined moments by simply matching the dimensionless coda derived moment $log_{10}A_0$ with the estimated seismic moment $log_{10}M_0$. The estimated $M_p$ values are given in Table 6.1.1. Once we have obtained the coda derived source spectra, the seismic moment $M_0$ *(coda)* is estimated by averaging the measurements of the moment rate spectra for frequencies lower than the estimated corner frequency. And the coda moment magnitude $M_w$ *(coda)* is then computed using the relation given by Hanks and Kanamori (1979):

$$M_w(coda) = \frac{2}{3}\log_{10} M_0(coda) - 10.75 \quad (5)$$

## 6.1.3 Results

### *6.1.3.1 Coda wave stability*

Fig. 6.1.8 shows direct S and coda waves interstation amplitudes before and after distance corrections. The interstation coda amplitude scatter is reduced after distance correction, which means that our distance normalization is a good approximation to the coda distance attenuation. Secondly, the distance corrected coda interstation standard deviation is usually lower than 0.1 whereas the direct-wave deviation is 3 to 4 times larger. This is consistent with previous studies (Morasca *et al.*, 2005; Mayeda and Walter, 1996).

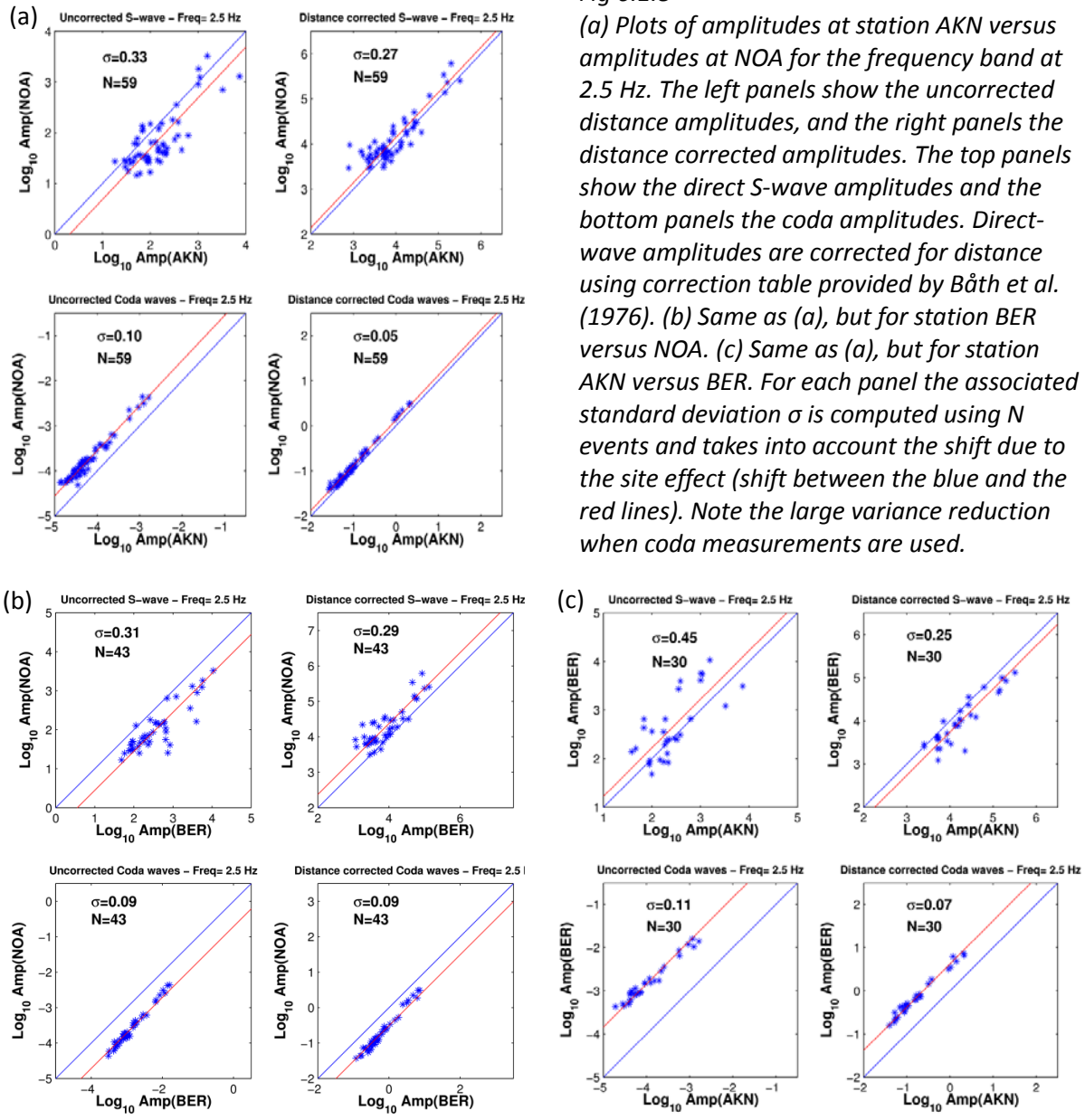


*Fig 6.1.8*
*(a) Plots of amplitudes at station AKN versus amplitudes at NOA for the frequency band at 2.5 Hz. The left panels show the uncorrected distance amplitudes, and the right panels the distance corrected amplitudes. The top panels show the direct S-wave amplitudes and the bottom panels the coda amplitudes. Direct-wave amplitudes are corrected for distance using correction table provided by Båth et al. (1976). (b) Same as (a), but for station BER versus NOA. (c) Same as (a), but for station AKN versus BER. For each panel the associated standard deviation σ is computed using N events and takes into account the shift due to the site effect (shift between the blue and the red lines). Note the large variance reduction when coda measurements are used.*

### *6.1.3.2 Moment source spectra*

Fig. 6.1.9 shows the S-wave power spectral density of four selected events in our database, all recorded by the same station AKN. Each spectrum has been instrument corrected. These four events are located in the same area in southwestern Norway (see Fig. 6.1.1), so we expect similar attenuation and other path effects for all. The top panels show displacement spectra of a confirmed explosion and a confirmed earthquake and the bottom panels correspond to two events of unknown origin (as reported in the Bergen seismic bulletin). Here, we have a relatively good illustration of the difference of spectral shape between earthquakes and explosions. Note that our power spectral density is not corrected by the attenuation or other path effects. The earthquake source spectrum is clearly characterized by a plateau of constant spectral amplitudes (see Fig 6.1.9.b), whereas the explosion source spectrum (Fig 6.1.9.a) has a deficiency in the high frequency content as compared with the earthquake. According to this observation, one of the unknown events is therefore explosion like (Fig. 6.1.9.c), whereas the other unknown event is more earthquake like (Fig. 6.1.9.d).

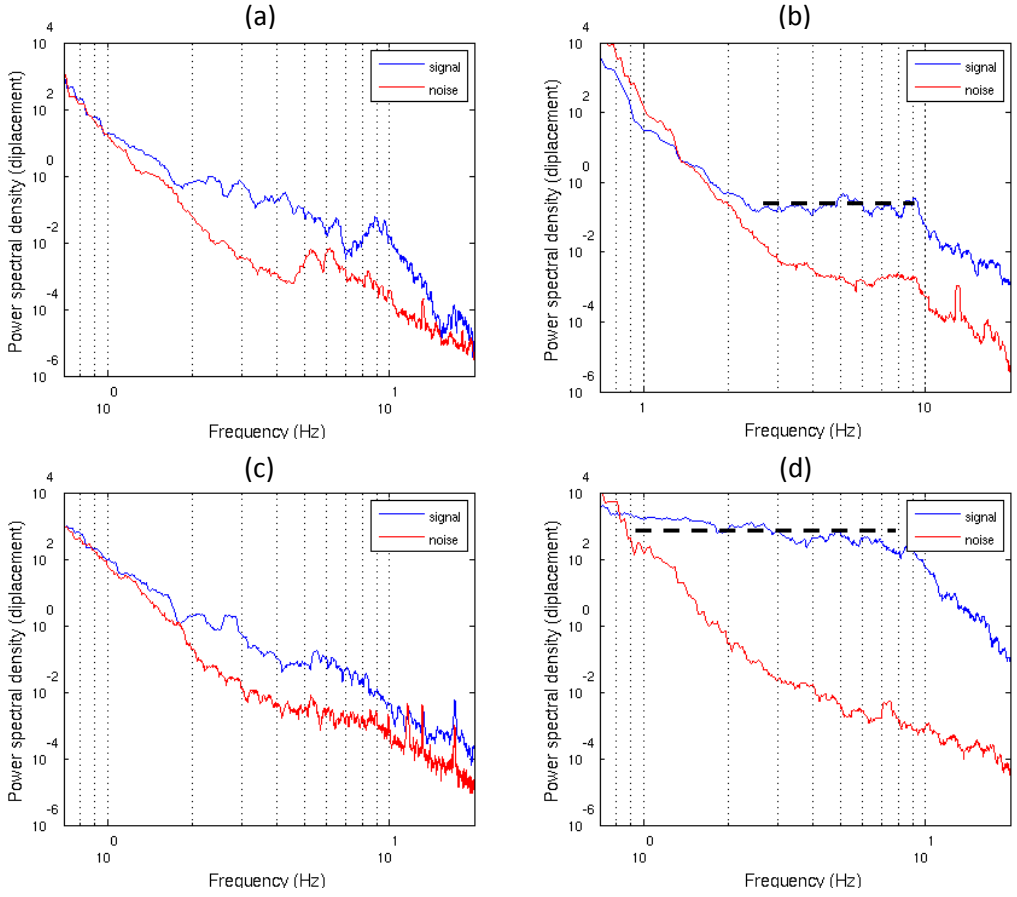


*Fig 6.1.9 Power spectral density of S-wave and noise windows for four selected events which are all recorded by AKN and occurred in the same area marked by a dotted circle in Fig. 6.1.1. All spectra have been corrected for instrument response, but not corrected for attenuation or other path effects. (a) Spectrum of a confirmed explosion. (b) Spectrum of a confirmed earthquake. (c) Spectrum of a suspected explosions (occurring during working hours with a source depth less than 5 km). (d) Spectrum of a suspected earthquake (occurring at night with a source depth greater than 10 km and a magnitude larger than 3). The dotted lines indicate a typical spectral plateau for earthquakes.*

Fig. 6.1.10 shows the coda derived source moment spectra at the three calibrated stations for all events listed in the Appendix. The site response corrections had been done twice, once using all events, and thereafter using only the events with earthquake-like ("normal") coda derived source moment spectra. The site response corrections are listed in Table 6.1.1.

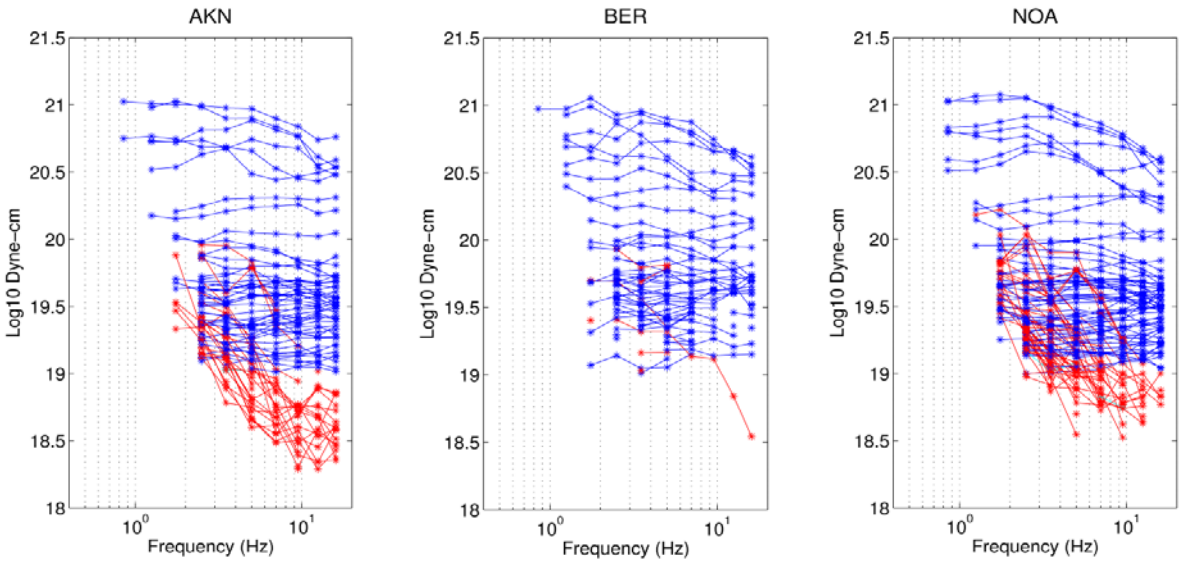


*Fig. 6.1.10 Coda derived source moment spectra estimated at the three different stations AKN, BER and NOA. Blue lines correspond to earthquake-like ("normal") spectra and red lines to explosion-like ("anomalous") spectra. The site response corrections are estimated using only selected events with "normal" spectra in order to remove bias introduced by man-made events.*

In Fig. 6.1.11, a number of coda-derived source moment spectra from common events are placed on top of each other showing the consistency of the estimates at the three stations.

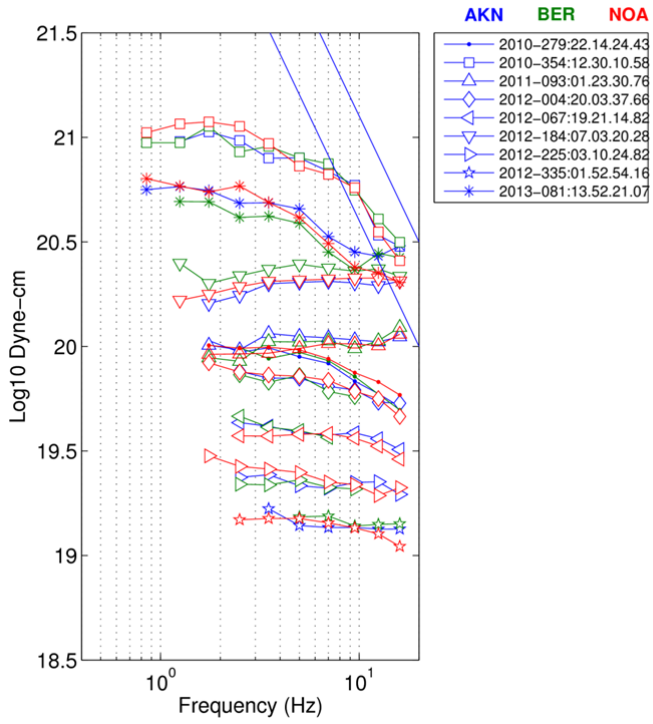


*Fig 6.1.11*
*Example of coda derived source moment spectra for common events at three different stations AKN (blue), BER (green) and NOA (red). Diagonal blue lines have a slope proportional to $f^{-2}$. Note that the estimates of the source spectrum at each of the three stations are very consistent for each of the events.*

### 6.1.3.3 Coda magnitude

The coda magnitude estimates from the three stations ($M_w(coda\text{-}AKN)$, $M_w(coda\text{-}BER)$ and $M_w(coda\text{-}NOA)$) are listed for each event listed in the Appendix. Notice that for a number of events it was not possible to do the coda analysis because of low signal-to-noise ratio or data quality problems at the recording station. For the station AKN data were not available before November 2009. Fig. 6.1.12 shows that $M_w(coda)$ estimates from different stations are in good agreement with interstation standard deviations below 0.15. This study shows very promising results for events larger than 2.25. We can see a larger scatter for the smaller events due to the fact that the coda length is shorter for these events. Mayeda *et al.* (2003) studied the dependence of coda length window with the amplitude measurement error. They show that the interstation scatter increases when using increasingly shorter window lengths and becomes quickly asymptotic to those of the direct waves as the window length approach the direct arrival. In any case the scatter for the smaller events will not be larger than the scatter we could have using the direct waves.

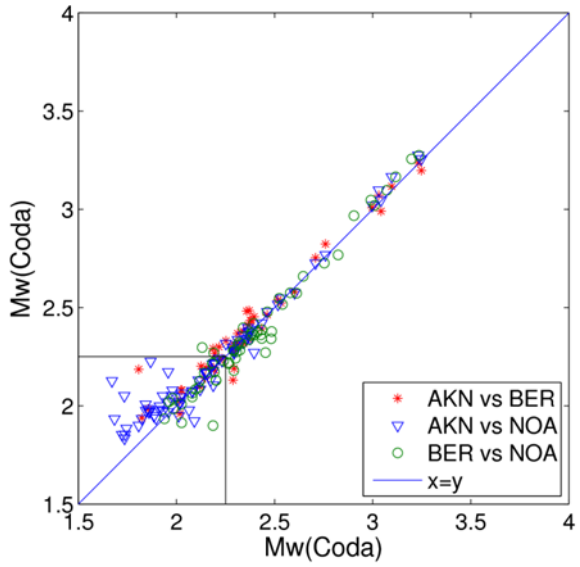


| | | σ | N |
|---|---|---|---|
| All Events | AKN-BER | 0.08 | 49 |
| | AKN-NOA | 0.10 | 83 |
| | BER-NOA | 0.07 | 61 |
| Events with MwCoda>2.25 | AKN-BER | 0.05 | 29 |
| | AKN-NOA | 0.04 | 32 |
| | BER-NOA | 0.06 | 36 |
| Events with MwCoda<2.25 | AKN-BER | 0.11 | 20 |
| | AKN-NOA | 0.13 | 51 |
| | BER-NOA | 0.08 | 25 |

*Fig. 6.1.12 Interstation scatter plot between stations AKN, BER and NOA obtained by plotting estimated moment magnitude from our coda-derived source spectra. The associated standard deviation σ is computed using N events.*

### 6.1.3.4 Events with anomalous spectra

The locations of events used in this study (yellow and blue filled circles) as well as the location of all probable and confirmed explosions reported in the Bergen catalog (stars) since 2009 are shown in Fig. 6.1.13. We note that most of events with anomalous coda derived source spectra (blue circles) are located in areas where explosions occur frequently. This is a strong indication that most of these "anomalous events" are man-made.

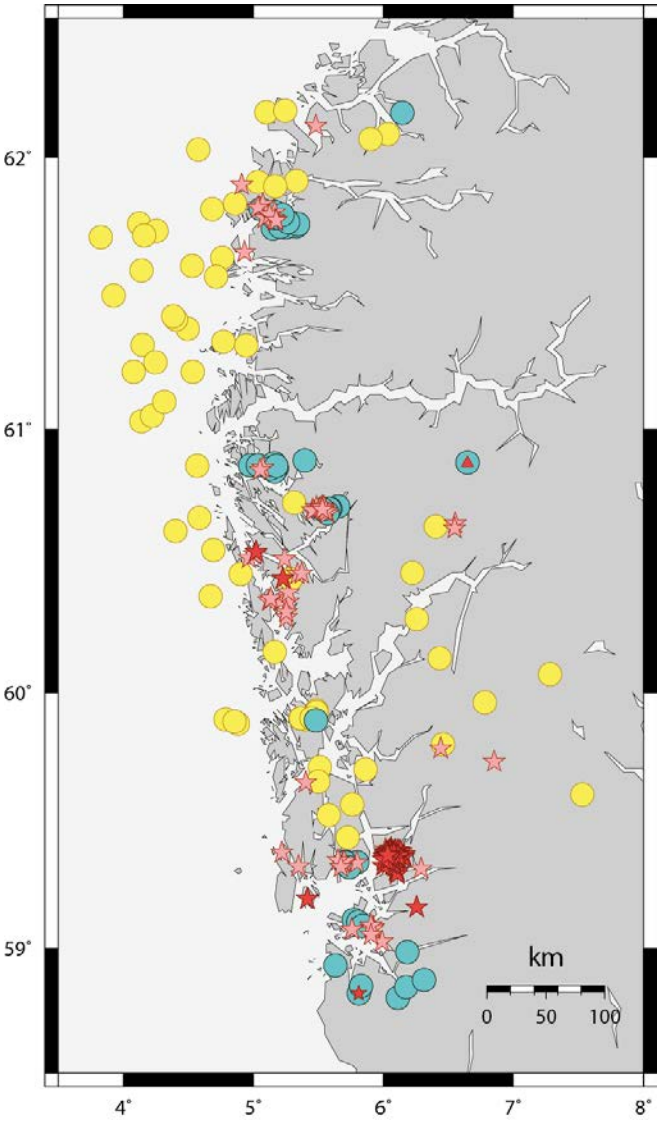


*Fig. 6.1.13*
*Events (filled circles) used in this study. Yellow circles correspond to events with normal coda-derived source spectra and blue circles to events with anomalous coda-derived source spectra. Small red triangles correspond to reported landslides. Pink and red stars, respectively, correspond to all probable and confirmed explosions since 2009 as reported in the Bergen catalog, also including events not used in this study. Notice that the basis for our study was events reported in the NORSAR catalog which is less complete than the Bergen catalog. Also note that most of events with anomalous coda derived source spectra are located in areas where explosions occur frequently.*

In order to further investigate the events with anomalous spectra, we have made time-of-day histograms of events used in this study, and of events since 2009 located in the same area as reported in the Bergen catalog (see Fig. 6.1.14). We first notice by separating out the explosions (yellow) an increase in the number of remaining events during the working hours, which means that our dataset as well as the Bergen catalog contain unidentified man-made events. We also notice from Fig. 6.3.14.a that the number of events with normal spectra remains relatively constant during all hours of the day whereas the events with anomalous spectra occur almost only during working hours, meaning that most of the "anomalous events" are likely to be man-made.

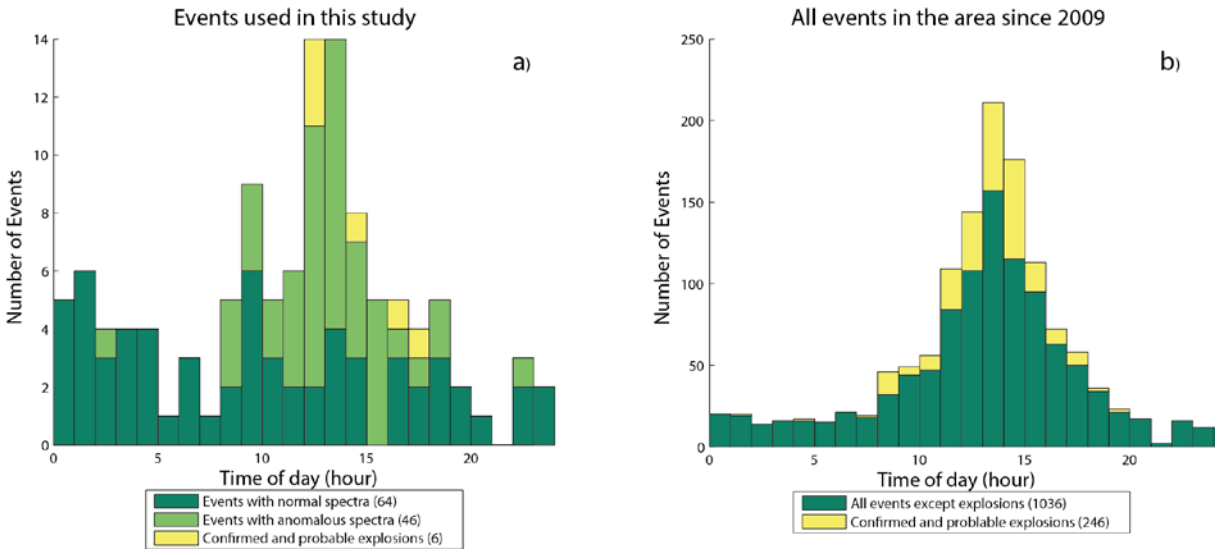


*Fig. 6.1.14 Histograms of events over the 24 hours of the day. (a) Histogram of events used in the study. (b) Histogram using all events since 2009 reported in the Bergen catalog.*

### 6.1.4 Summary and suggestions for improvements

As confirmed by this study, coda amplitude measurements are significantly more consistent between stations than amplitude measurements of the direct wave. The use of regional coda envelopes for estimation of source moment spectra and event magnitudes of events in Norway is promising. Indeed, a coda based procedure permits quite accurate estimation of moment magnitudes for events observed at a few stations only. For Norway, where the seismicity is characterized as low-to-intermediate with a large offshore component, this is very advantageous as a large fraction of the events are recorded at relatively few stations. In contrast, classical estimates of moment magnitudes require observation at a relatively large number of stations.

A natural follow-up to this study would be to calibrate other regions and stations and to estimate the magnitude uncertainty as proposed by Mayeda (2003). In connection with the estimation of coda magnitudes for older, and possibly also clipped events, in the NORSAR and Bergen catalogs, it would be interesting to investigate the use of 1-D or 2-D path corrections.

In this study, only the vertical component data has so far been used. We also suggest investigating the additional use of the horizontal components where we in many cases expect more S-wave energy than on the verticals.

The analytic expression of coda envelopes is known to fit long cods poorly. Many investigations found lapse time dependence of the coda decay rate which suggests that the later portion of the coda is dominated by energy that has propagated in zones with different attenuation characteristics than the energy in the early coda (Sato *et al*., 2009). It would thus be interesting to restrict the length of the coda window to avoid this effect and only use the early coda for fitting of the synthetic envelopes. Another alternative would be to introduce a lapse time dependence of the coda decay, by using a polynomial regression instead of linear regression.

Another improvement would be to better classify and eliminate man-made events from the event population prior to the estimation of the site response corrections. In this study, the site response corrections was done twice, first using all events, and then after discarding events having anomalous coda derived source moment spectra. Phillips *et al.*, (2008) suggest a procedure using only events with magnitudes below 3 that occurred at night, or with reliable source depths below 5 km. Further improvements to the separation of earthquakes from man-made events could *e.g.*, be made by analyzing the time-domain and/or frequency-domain characteristics of the waveforms.

**C. Labonne**
**T. Kværna**
**M. Roth**

***References***

Aki, K., and B.Chouet (1975). Origin of Coda Waves: Source, Attenuation and Scattering Effects. *J. Geophys. Res*. **80**, 23, 3322-3342.

Bormann, P. (Ed.) (2002). New Manual of Seismological Observatory Practice (NMSOP-1), IASPEI, GFZ German Research Centre for Geosciences, Potsdam.

Båth, M., O. Kulhanek, T. Van Eck and R. Wahlstrøm (1976). Engineering analysis of ground motion in Sweden, *Report No 5-76*, Seismological Institute, Uppsala, Sweden, 59 pp.

Eken, T., K. Mayeda, A. Hofstetter, R. Gök, G. Örgülü and N.i Turkelli (2004). An application of the coda methodology for moment-rate spectra using broadband stations in Turkey. *Geophys. Res. Lett.* **31**.

Hanks, T. C. and H. Kanamori (1979). A moment magnitude scale. *J. Geophys. Res*., **84**, 2348-2350

Mayeda, K. and W. R. Walter (1996). Moment, energy, stress drop, and source spectra of western United States earthquakes from regional coda envelopes. *J. Geophys. Res.* **101**, 11,195-11,208.

Mayeda, K., A. Hofstetter, J. L. O'Boyle and W.R. Walter (2003). Stable and Transportable Regional Magnitudes Based on Coda-Derived Moment-Rate Spectra. *Bull. Seism. Soc. Am,.* **93** , 224-239.

Morasca, P., K. Mayeda, L. Malagnini and W.R. Walter (2005). Coda-derived source spectra, moment magnitudes and energy-moment scaling in the western Alps. *Geophys. Res. Lett*., **32**, no. 22.

Morasca, P., K. Mayeda, R. Gök and L. Malagnini (2008). Source effects from broad area network calibration of regional distance coda waves. *Bull. Seism. Soc. Am*. **98**, 1936-1946.

Phillips, W.S., R.J. Stead, G.E. Randall, H.E. Hartse and K.M. Mayeda (2008). Earth Heterogeneity and Scattering Effects on Seismic Waves. In: *Advances in Geophysics*, vol 50, Chapter 12, Source effects from broad area network calibration of regional distance coda waves.

Ringdal, F. (1983). Magnitudes from P coda and Lg using NORSAR data. In NORSAR Semiannual Technical Summary, 1 October 82-31 March 83, *NORSAR Sci. Rep. No. 2-82/83*, NTNF/NORSAR, Kjeller, Norway.

Ringdal, F. Hokland, B. K. (1987). Magnitudes of large Semipalatinsk explosions using P coda and Lg measurements at NORSAR. In Semiannual Technical Summary, 1 April-30 September 1987, *NORSAR Sci. Rep. 1-87/88*, Kjeller, Norway.

Sato, H., M. C. Fehler and T. Maeda (2009). Seismic wave propagation and scattering in the heterogeneous Earth. Chapter 2.4, Scattering of high-frequency seismic waves. *Springer-Verlag Berlin Heidelberg*. 19-40

# Appendix

***Origin time, latitude, longitude and depth of events used in this study, with event label as provided in the Bergen bulletin (L for local event, LE for confirmed local explosion, LX for landslide and LQ for confirmed earthquakes), label of the obtained spectrum (A for Anomalous, N for Normal, and U for Unknown), the corresponding local magnitude from NORSAR, local magnitude from Bergen, moment magnitude from Bergen, and the estimated coda magnitudes from AKN, BER and NOA.***

| T0 | Lat | Lon | Depth | Event Label | Spectrum Label | $M_L$ | $M_L$ | $M_W$ | $M_{coda}$ | $M_{coda}$ | $M_{coda}$ |
|---|---|---|---|---|---|---|---|---|---|---|---|
| YYYY-DOY:HH.MM.SS.S | (°) | (°) | (km) | | | NOA | BER | BER | AKN | BER | NOA |
| 2009-008:14.27.26.2 | 60.71 | 5.652 | 0 | L | A | 1.58 | 1.4 | - | - | - | 1.907 |
| 2009-040:23.31.09.9 | 60.157 | 5.165 | 15 | L | N | - | 1.8 | - | - | - | 1.962 |
| 2009-049:12.03.51.9 | 58.801 | 6.11 | 15 | L | A | 1.93 | 2.0 | - | - | - | 2.208 |
| 2009-088:02.39.52.7 | 62.16 | 6.144 | 15 | L | A | 2.53 | 2.1 | - | - | - | 2.268 |
| 2009-113:09.18.47.7 | 61.754 | 5.215 | 15 | L | A | 2.07 | - | - | - | - | - |
| 2009-132:15.16.57.8 | 60.436 | 5.23 | 0.0F | LE | - | 1.64 | 1.7 | - | - | - | - |
| 2009-136:16.41.51.3 | 59.71 | 5.513 | 0.1 | L | N | 2.28 | 2.3 | - | - | 2.385 | 2.369 |
| 2009-139:04.16.36.6 | 62.162 | 5.1 | 13.0F | L | N | - | 3.0 | 3.0 | - | 2.904 | 2.968 |
| 2009-148:14.08.25.7 | 60.702 | 5.592 | 0 | L | U | - | 1.3 | - | - | - | 1.774 |
| 2009-154:12.57.30.2 | 61.748 | 5.275 | 15.0F | L | A | 2.18 | 2.2 | - | - | - | 2.305 |
| 2009-156:12.28.06.6 | 58.842 | 5.822 | 0 | L | A | 1.62 | 1.7 | - | - | - | 2.022 |
| 2009-158:17.30.56.7 | 60.132 | 6.433 | 3 | L | N | 1.74 | 1.9 | - | - | 2.117 | 2.127 |
| 2009-170:09.45.26.2 | 58.845 | 6.177 | 15.0F | L | A | 1.89 | 1.7 | - | - | - | 2.014 |
| 2009-184:01.12.03.6 | 62.084 | 6.033 | 2.4 | L | N | 1.87 | 1.7 | - | - | 1.980 | 2.039 |
| 2009-211:12.44.44.5 | 61.748 | 5.332 | 15.0F | L | A | 1.95 | 1.8 | - | - | - | 2.082 |
| 2009-223:12.39.54.8 | 58.872 | 6.312 | 3.5 | L | A | 1.69 | 1.7 | - | - | - | 2.022 |
| 2009-237:12.26.02.2 | 61.74 | 5.152 | 15.0F | L | A | 2.18 | 2.0 | - | - | - | 2.302 |
| 2009-238:18.19.47.2 | 61.91 | 5.037 | 17.3 | L | N | 2.17 | 2.1 | 2.4 | - | 2.430 | 2.361 |
| 2009-239:18.27.49.9 | 60.864 | 4.976 | 0.1 | L | A | 1.54 | 1.3 | - | - | - | 1.979 |
| 2009-253:09.07.54.9 | 61.71 | 3.825 | 18.1 | L | N | 2.57 | 2.7 | 2.7 | - | 2.646 | 2.660 |
| 2009-257:00.39.48.4 | 60.667 | 4.585 | 15 | L | N | 2.34 | 2.6 | 2.5 | - | 2.619 | 2.573 |
| 2009-282:08.11.55.2 | 61.745 | 5.244 | 0 | L | A | 2.19 | 2.0 | - | - | - | 2.282 |
| 2009-288:10.13.57.3 | 59.326 | 5.735 | 0 | L | A | 1.57 | 1.8 | - | - | - | 2.007 |
| 2009-289:09.37.35.7 | 61.373 | 4.495 | 0 | L | N | 1.87 | - | - | - | - | - |
| 2009-297:16.18.19.6 | 61.407 | 4.406 | 1.6 | L | N | 1.83 | 1.8 | - | - | 2.113 | 2.093 |
| 2009-301:06.09.53.4 | 59.703 | 5.861 | 12.3 | L | N | 2.54 | 2.2 | 2.6 | - | 2.394 | 2.359 |
| 2009-303:03.42.38.2 | 61.313 | 4.147 | 20.2 | L | N | 1.85 | 2.0 | - | - | 2.263 | 2.215 |
| 2009-308:12.52.28.1 | 59.328 | 5.711 | 2 | L | A | 1.74 | 1.9 | - | - | - | 2.023 |
| 2009-310:11.35.46.3 | 60.701 | 5.594 | 0 | L | A | 2.09 | 1.6 | - | 1.978 | - | 2.079 |
| 2009-344:12.49.14.9 | 60.714 | 5.622 | 0 | L | U | 1.60 | 1.6 | - | 1.932 | - | 1.975 |
| 2009-344:13.03.14.1 | 61.746 | 5.205 | 0 | L | A | 1.80 | 1.7 | - | 1.868 | - | 2.226 |
| 2010-031:00.04.28.0 | 61.588 | 4.139 | 12.3 | L | N | 2.42 | 2.2 | - | 2.383 | 2.435 | 2.387 |
| 2010-036:13.26.17.1 | 61.812 | 5.055 | 0 | L | A | 2.17 | 1.9 | - | 1.930 | - | 2.050 |

| | | | | | | | | | | | |
|---|---|---|---|---|---|---|---|---|---|---|---|
| 2010-041:06.04.35.6 | 59.8 | 6.46 | 12.0F | L | N | 2.31 | 2.2 | 2.5 | 2.365 | 2.340 | 2.397 |
| 2010-060:00.41.48.0 | 62.027 | 4.576 | 10.0F | L | N | 2.07 | 2.1 | 2.5 | 2.343 | 2.318 | 2.323 |
| 2010-062:15.54.23.1 | 58.819 | 5.809 | 0.0F | LE | A | 1.85 | 1.9 | - | 2.063 | - | 1.978 |
| 2010-063:14.36.17.7 | 59.34 | 5.708 | 0 | L | A | 1.63 | 1.6 | - | 2.091 | - | 1.923 |
| 2010-067:13.18.37.8 | 61.762 | 5.287 | 0 | L | A | 1.64 | 1.5 | - | 1.737 | - | 1.854 |
| 2010-084:15.22.20.1 | 58.848 | 5.828 | 0 | L | A | 1.61 | 1.7 | - | 1.896 | - | 1.937 |
| 2010-085:13.05.54.0 | 61.782 | 5.158 | 0 | L | A | 1.86 | 1.7 | - | 1.855 | 1.983 | 1.984 |
| 2010-096:11.29.11.4 | 61.779 | 5.197 | 5.0F | L | A | 1.89 | 1.8 | - | 2.079 | - | 2.076 |
| 2010-099:13.02.08.5 | 60.7 | 5.584 | 0 | L | A | 1.97 | 1.5 | - | 1.858 | - | 1.974 |
| 2010-124:09.53.50.4 | 60.281 | 6.258 | 0 | L | N | 1.72 | 1.6 | - | 1.978 | - | 2.052 |
| 2010-127:17.54.06.7 | 61.812 | 4.684 | 13 | L | N | 2.25 | 2.3 | 2.5 | 2.433 | 2.394 | 2.420 |
| 2010-155:14.30.40.4 | 60.683 | 5.572 | 0.0F | LP | A | 1.66 | 1.5 | - | 2.187 | - | 2.104 |
| 2010-166:04.22.04.1 | 60.874 | 6.646 | 0.0F | LX | A | 2.11 | 1.5 | - | 1.915 | - | 1.998 |
| 2010-167:08.47.22.6 | 61.757 | 5.345 | 4.5 | L | A | 1.75 | 1.0 | - | 1.744 | - | 1.885 |
| 2010-185:17.40.49.6 | 61.802 | 5.165 | 0.0F | LP | A | 1.59 | 1.8 | - | 1.845 | - | 1.975 |
| 2010-187:12.40.18.7 | 59.338 | 5.799 | 0.0F | LP | A | 1.67 | 1.6 | - | - | - | 2.005 |
| 2010-210:04.32.27.2 | 61.028 | 4.137 | 17.3 | L | N | 1.98 | 2.0 | - | 2.233 | 2.240 | 2.229 |
| 2010-213:02.59.58.4 | 62.067 | 5.899 | 15.0F | L | N | 1.97 | 2.0 | - | 2.293 | 2.189 | 2.270 |
| 2010-220:23.23.28.3 | 62.168 | 5.245 | 1.9 | L | N | 1.63 | 1.7 | - | 2.12 | 2.096 | 2.084 |
| 2010-259:11.57.36.4 | 59.338 | 5.705 | 0.0F | LP | A | 1.50 | 1.6 | - | 2.011 | - | 1.949 |
| 2010-264:10.13.21.5 | 61.049 | 4.221 | 8.8 | L | N | 2.26 | 1.8 | - | 1.956 | - | 2.019 |
| 2010-273:12.51.33.3 | 60.368 | 4.67 | 12.5 | L | N | 2.10 | 2.3 | - | 2.370 | 2.485 | 2.378 |
| 2010-279:22.14.24.6 | 61.42 | 4.385 | 10.0F | L | N | 2.73 | 2.3 | - | 2.533 | 2.524 | 2.547 |
| 2010-281:04.08.32.7 | 59.604 | 7.531 | 15.0F | L | N | 1.79 | 1.5 | - | 2.112 | - | 2.13 |
| 2010-286:13.18.40.2 | 60.855 | 5.16 | 6.9 | L | A | 1.72 | 1.3 | - | 1.734 | - | 2.050 |
| 2010-316:15.16.01.1 | 60.853 | 5.132 | 0 | L | A | 1.96 | 1.4 | - | 1.86 | - | 1.968 |
| 2010-344:15.14.55.6 | 58.931 | 5.632 | 0 | L | A | 1.69 | 1.8 | - | 1.915 | - | 1.98 |
| 2010-349:12.34.28.9 | 59.319 | 5.74 | 0 | L | A | 1.77 | 1.8 | - | 1.842 | - | 2.007 |
| 2010-354:00.43.23.2 | 59.901 | 5.359 | 8.0F | L | N | 3.13 | 3.0 | 3.0 | 3.031 | 3.072 | 3.097 |
| 2010-354:00.51.18.8 | 59.899 | 5.447 | 8.0F | L | N | 2.07 | 2.2 | 2.3 | 2.340 | 2.379 | 2.357 |
| 2010-354:00.59.31.5 | 59.93 | 5.486 | 12.0F | L | N | 1.58 | 1.8 | 1.9 | 2.027 | 2.080 | 2.063 |
| 2010-354:01.39.20.1 | 59.896 | 5.401 | 15 | L | N | 2.29 | 2.2 | 2.3 | 2.312 | 2.368 | 2.336 |
| 2010-354:12.30.12.7 | 59.9 | 5.366 | 17.0F | L | N | 3.36 | 3.3 | 3.3 | 3.232 | 3.235 | 3.275 |
| 2010-354:12.37.38.3 | 59.924 | 5.483 | 10.0F | L | N | 1.73 | 2.0 | 2.1 | 2.195 | 2.267 | 2.220 |
| 2010-354:12.53.39.4 | 59.9 | 5.446 | 15 | LQ | N | 1.61 | 1.7 | - | 1.959 | - | 1.969 |
| 2010-361:08.57.22.6 | 61.495 | 3.926 | 13.1 | L | N | 2.13 | 2.2 | - | 2.294 | 2.307 | 2.274 |
| 2011-016:22.43.04.3 | 59.892 | 5.482 | 12.0F | L | A | - | 1.7 | - | - | 2.026 | 1.914 |
| 2011-037:08.02.29.2 | 61.832 | 4.858 | 15 | L | N | 1.83 | 1.7 | - | 2.174 | 2.200 | 2.131 |
| 2011-037:18.41.39.8 | 60.723 | 5.312 | 29 | L | N | 1.87 | 1.8 | - | 2.217 | 2.300 | 2.241 |
| 2011-082:14.45.53.6 | 59.369 | 6.072 | 0.0F | L | A | 2.12 | 2.2 | - | 2.376 | 2.434 | 2.3430 |
| 2011-088:11.30.38.0 | 59.111 | 5.774 | 0 | L | A | 2.27 | 2.1 | - | 2.395 | 2.453 | 2.271 |
| 2011-090:13.00.26.9 | 59.104 | 5.808 | 0 | L | A | 2.44 | 2.3 | - | 2.358 | 2.483 | 2.341 |
| 2011-093:01.23.30.9 | 61.101 | 4.315 | 16.2 | L | N | 2.45 | 2.4 | - | 2.602 | 2.580 | 2.575 |
| 2011-095:12.30.02.0 | 59.088 | 5.84 | 0 | L | A | 2.23 | 2.2 | - | - | 2.411 | 2.375 |
| 2011-118:22.24.07.4 | 59.96 | 6.78 | 12.0F | L | N | 2.01 | 2.0 | - | 2.193 | 2.184 | 2.217 |
| 2011-186:01.22.44.8 | 60.863 | 4.568 | 17.4 | L* | N | 2.12 | 2.4 | - | 2.365 | 2.411 | 2.375 |

| | | | | | | | | | | | |
|---|---|---|---|---|---|---|---|---|---|---|---|
| 2011-273:12.47.26.3 | 60.699 | 5.533 | 0.0F | LP | A | 1.90 | 1.6 | - | - | - | 2.245 |
| 2011-317:02.39.16.5 | 60.435 | 5.29 | 11.1 | L | N | 1.93 | 2.0 | 2.0 | 2.187 | 2.292 | 2.179 |
| 2011-359:14.49.23.6 | 61.214 | 4.08 | 22.9 | L | N | 2.04 | 1.9 | - | 2.191 | 2.182 | 2.215 |
| 2011-365:00.16.17.3 | 61.635 | 4.762 | 1 | L | N | 2.40 | 2.1 | - | 2.314 | 2.313 | 2.309 |
| 2012-004:20.03.37.8 | 61.758 | 4.12 | 15 | L | N | 2.42 | 2.4 | - | 2.462 | 2.463 | 2.478 |
| 2012-067:19.21.17.4 | 61.915 | 5.331 | 15 | L | N | 1.94 | 2.0 | - | 2.304 | 2.324 | 2.284 |
| 2012-074:09.15.55.7 | 61.895 | 5.17 | 15 | L | N | 2.07 | 2.1 | - | 2.364 | - | 2.357 |
| 2012-074:19.22.27.9 | 59.524 | 5.578 | 13.7 | L | N | 3.07 | 3.2 | - | 3.097 | 3.117 | 3.166 |
| 2012-075:04.10.14.1 | 59.566 | 5.761 | 0 | L | N | 1.87 | 2.2 | - | 2.297 | 2.289 | 2.281 |
| 2012-084:06.05.18.2 | 60.616 | 4.399 | 15.0F | L | N | 2.64 | 2.9 | - | 2.708 | 2.753 | 2.726 |
| 2012-084:11.06.30.5 | 60.634 | 6.401 | 15.3 | L | N | 3.16 | 3.0 | - | 2.997 | 3.009 | 3.020 |
| 2012-117:05.18.28.8 | 60.07 | 7.282 | 0 | L | N | 1.93 | 1.9 | - | 2.184 | - | 2.212 |
| 2012-146:14.02.27.3 | 61.732 | 4.256 | 2.5 | L | N | 1.94 | 2.0 | - | 2.289 | 2.293 | 2.281 |
| 2012-166:13.35.17.4 | 58.827 | 6.231 | 0.0F | LE | - | 1.82 | - | - | - | - | - |
| 2012-169:09.08.59.2 | 58.983 | 6.184 | 0 | L | A | 2.27 | 2.1 | - | 2.288 | 2.131 | 2.297 |
| 2012-184:07.03.21.3 | 60.458 | 6.223 | 0 | L | N | 2.70 | 2.9 | - | 2.759 | 2.823 | 2.768 |
| 2012-216:02.55.51.2 | 60.544 | 4.69 | 2.1 | L | N | 1.66 | 1.8 | - | 2.022 | 2.080 | 2.045 |
| 2012-225:03.10.23.9 | 61.249 | 4.247 | 4 | L | N | 2.03 | 1.8 | - | 2.146 | 2.141 | 2.168 |
| 2012-227:07.21.30.8 | 60.442 | 6.023 | 15 | L | - | 1.59 | - | - | - | - | - |
| 2012-258:08.03.09.1 | 60.853 | 5.133 | 0 | L | A | 1.64 | 1.5 | - | - | - | 1.965 |
| 2012-264:17.32.25.7 | 60.853 | 5.182 | 0.1 | L | A | 1.67 | 1.5 | - | 1.822 | - | - |
| 2012-286:13.01.43.9 | 60.857 | 5.161 | 0 | L | A | 1.67 | 1.5 | - | 1.722 | - | 1.853 |
| 2012-298:13.47.48.7 | 61.325 | 4.768 | 15 | L | N | 1.60 | 1.6 | - | 2.082 | - | 2.074 |
| 2012-314:10.07.14.3 | 61.765 | 5.265 | 0.1 | L | A | 1.72 | 1.8 | - | 1.885 | - | 1.949 |
| 2012-335:01.52.53.4 | 61.31 | 4.944 | 0 | L | N | 1.76 | 1.7 | - | 2.015 | 2.025 | 2.008 |
| 2012-345:13.06.53.2 | 59.654 | 5.498 | 0 | L | N | 2.05 | 1.8 | - | 2.149 | 2.193 | 2.173 |
| 2012-360:11.06.09.2 | 61.716 | 4.162 | 0.3 | L | N | 1.57 | 1.7 | - | 2.017 | 1.961 | 2.020 |
| 2013-023:17.42.32.3 | 61.213 | 4.535 | 23.6 | L | N | 2.03 | 2.1 | - | 2.252 | 2.331 | 2.317 |
| 2013-057:09.21.49.4 | 60.454 | 4.901 | 18.7 | L | N | 1.98 | - | - | - | - | - |
| 2013-066:16.07.29.4 | 60.865 | 5.033 | 0 | L | A | 1.86 | - | - | - | - | - |
| 2013-079:15.00.35.4 | 60.873 | 5.158 | 0.1 | L | A | 1.62 | 1.4 | - | 1.807 | 2.186 | 1.899 |
| 2013-081:10.32.44.5 | 61.566 | 4.714 | 15 | L | N | 3.36 | 3.0 | 3.3 | 3.248 | 3.198 | 3.257 |
| 2013-081:13.52.21.9 | 61.603 | 4.528 | 0 | L | N | 3.18 | 2.7 | 3.1 | 3.042 | 2.991 | 3.048 |
| 2013-092:15.02.57.8 | 60.848 | 5.163 | 0 | L | A | 1.69 | 1.4 | - | 1.735 | - | 1.834 |
| 2013-098:02.17.35.3 | 59.897 | 4.788 | 10.0F | L | N | 1.77 | 1.9 | - | 2.125 | 2.201 | 2.129 |
| 2013-101:16.10.06.3 | 61.792 | 5.222 | 0 | L | A | 1.77 | 1.8 | - | 1.958 | - | 2.172 |
| 2013-114:14.02.43.0 | 60.882 | 5.396 | 0 | L | A | 1.60 | 1.3 | - | 1.692 | - | - |
| 2013-144:12.07.08.4 | 60.842 | 5.163 | 0 | L | A | 1.65 | 1.3 | - | 1.671 | - | 2.126 |
| 2013-150:14.04.41.8 | 60.851 | 5.131 | 0.1 | L | A | 1.66 | 1.3 | - | 1.823 | 1.938 | 1.934 |
| 2013-154:16.37.27.9 | 59.436 | 5.726 | 5.8 | L | N | 2.54 | 2.5 | - | 2.517 | 2.540 | 2.516 |
| 2013-157:08.15.47.7 | 59.879 | 4.88 | 0 | L | N | 1.61 | 1.6 | - | 2.015 | - | 2.012 |
| 2013-158:09.15.21.9 | 59.888 | 4.853 | 0 | L | N | 1.90 | 1.8 | - | 2.159 | - | 2.165 |
| 2013-162:18.03.31.0 | 60.863 | 5.175 | 0 | L | A | 1.71 | 1.5 | - | 1.684 | - | 1.933 |